Remote Sensing Applications: Society and Environment 4 (2016) 211–218

Contents lists available at ScienceDirect

Remote Sensing Applications: Society and Environment

journal homepage: www.elsevier.com/locate/rsase

Estimation of above ground forest biomass at Muğla using ICESat/GLAS and Landsat data

Doğukan Doğu Yavaşlı

Ahi Evran University Department of Geography, Kırşehir, Turkey

ARTICLE INFO

Keywords:
Forest biomass
ICESat
GLAS
Landsat
Muğla

ABSTRACT

Accurate estimation of aboveground forest biomass (AGB) is essential for carbon budgets. In this study we present the use of both satellite lidar (ICESat/GLAS) and optical (Landsat) data for estimation of AGB at Muğla province of Turkey. We collected field data in 2013 and 2014. Plot-level AGB estimates were calculated using equations representative to the species at the study area. Various GLAS parameters and Landsat vegetation indices were modeled using multiple regression analysis to estimate AGB. In the first model ($Model_1$) height of median energy (HOME) and the ratio of HOME to maximum vegetation height (%HOME) parameter of GLAS showed relation with field based AGB estimates with a coefficient of determination (R^2) of 0.88. The second model ($Model_2$) that uses the AGB estimations of $Model_1$ and the variables obtained from Landsat TM indices had a R^2 of 0.73. The resulting map was validated with field measurements and it has been found that calculation of AGB using $Model_1$ and $Model_2$ allows us to explain 79% of the variability of AGB at the study area with a RMSE of ± 28.16 t/ha. This study is the very first study on estimation of above ground forest biomass across Turkey, using a Lidar sensor, ICESat/GLAS with the combination of an optical system, Landsat. The results presented in this paper provide an example of the ability to use ICESat/GLAS waveforms and Landsat imagery for assessing aboveground biomass at the areas where airborne lidar data is not widely available.

1. Introduction

Biomass, along with various definitions, is generally used for the biological material consisting of vegetative organisms that grow through photosynthesis. With the process of photosynthesis, forests remove carbon dioxide from the atmosphere and store it in their biomass as carbon-containing chemical compounds (Sarker, 2010). This carbon returns to atmosphere as CO_2 by way of processes such as combustion and decomposition.

Most of the biomass assessment studies conducted are focused on aboveground forest biomass because it explains the majority of the total accumulated biomass in the forest ecosystem. Even though the organic matter in the soils may contain 2–3 times more carbon than aboveground biomass (AGB), the carbon in soils is protected both physically and chemically and cannot be oxidized easily apart from exceptional circumstances such as burning of peat (Davidson and Janssens, 2006). However, AGB is unguarded to fires, logging, climatic effects and the changes in land use activities therefore the available carbon can be easily released to the atmosphere.

There are various methods to estimate the biomass in a given area. Conventionally it is estimated by harvesting all plant material within a plot, drying and weighing it. Remote sensing techniques provide an alternative to this conventional method in estimating or monitoring or verifying an area of and biomass production or growth rates (Das and Ravindaranth, 2012). The advantages of using remote sensing over traditional field inventory methods for biomass estimation have been mentioned by a large number of publications (Sader et al., 1989; Roy and Ravan, 1996; Steininger, 2000; Lu, 2006; Ghasemi et al., 2011; Kumar et al., 2015). These include to collect data easily in areas which are difficult to access on the ground, to reduce the number of required fieldworks and thereby the costs, the speed with which remotely sensed data can be collected and processed.

Even though remotely sensed observations do not directly measure biomass, the radiometry is sensitive to vegetation structure (crown size and tree density), texture and shadow, which can be correlated with AGB (Baccini et al., 2008). Most recently, light detection and ranging (Lidar) and radio detection and ranging (Radar) remote sensing has been successfully used to characterize vegetation vertical structure and height, and to infer AGB.

Lidar is an active remote sensing technology, which emits laser pulses from the instrument towards a target and measures the reflected energy and/or time difference between the pulse emission and reception (Yavaşlı, 2012). Lidar systems can be grouped into two categories: discrete return and full waveform systems. Discrete return systems

E-mail address: dogukan.yavasli@ahievran.edu.tr.

http://dx.doi.org/10.1016/j.rsase.2016.11.004
Received 20 April 2016; Received in revised form 26 September 2016; Accepted 11 November 2016
Available online 13 November 2016

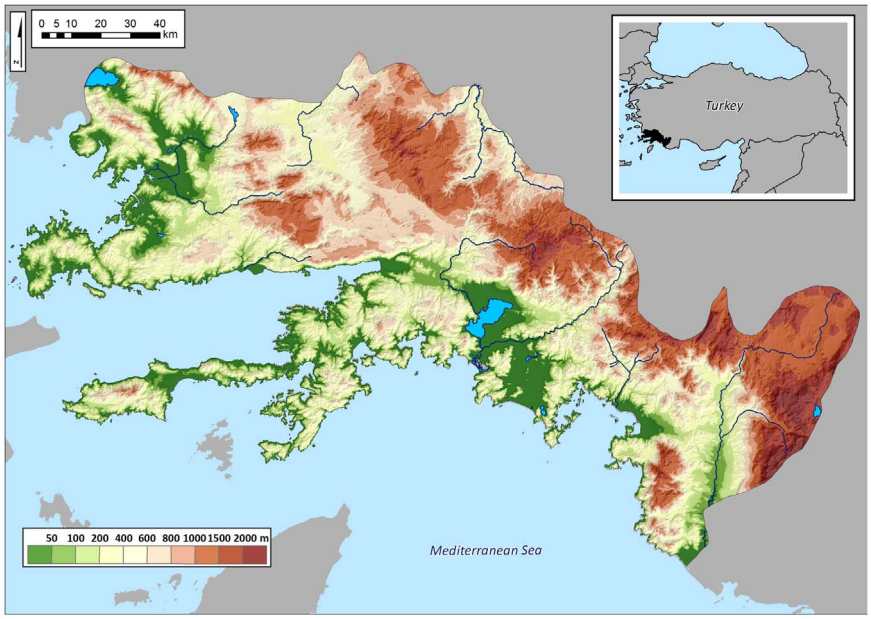

Fig. 1. Study area – Muğla province, Turkey.

record first and last returns or at times, also a number of intermediate points (Rosette et al., 2012) while full waveform lidar systems record the entire returned signal above a background energy noise threshold that is related to the vertical distribution of canopy structure (Dubayah and Drake, 2000).

AGB estimations with full waveform lidar systems such as the Geoscience Laser Altimeter System (GLAS) on Ice, Cloud, and Land Elevation Satellite (ICESat) provide information about the vertical structure of its "footprint" area of ~70 m diameter depending on intercepted surface area, orientation, surface reflectivity and the returned energy level changes in given height. The returned waveforms from the footprints can be used to estimate tree height, AGB, and basal area (Lefsky et al., 2007; Sun et al., 2008; Rosette et al., 2008), however accuracies depend on canopy density and terrain topography. More Recently, Zolkos et al. (2013) compared 70 AGB studies and indicated that AGB models using airborne lidar metrics are significantly more accurate than those based on the satellite-borne GLAS instrument, while the spatial extent of airborne lidar is typically restricted to relatively smaller areas. They have associated the difference in model accuracy to the sparse sampling density of GLAS which requires data fusion with other imagery.

Various studies have indicated that GLAS data can be used to achieve large-scale monitoring of AGB explaining 55% to %74 of the field estimates. (Lefsky et al., 2005; Boudreau et al., 2008; Pflugmacher et al., 2008; Zhang et al., 2008; Fu et al., 2009; Guo et al., 2010). For instance, Lefsky et al. (2005) combined ICESat waveforms and ancillary topography from the Shuttle Radar Topography Mission (SRTM) to estimate AGB of tropical broadleaf forests in Brazil and the model explained 73% of the field-estimates. Similarly, Boudreau et al. (2008) have shown that GLAS data with the combination of SRTM data can be used to achieve large-scale monitoring of AGB at the northern forests of Québec with an R^2 of 0.59. Guo et al. (2010) have estimated AGB for forests in Daxinganlin in northeastern China by combining HJ-1 satellite data with GLAS and have achieved R^2 of 0.71. A more comprehensive review of AGB estimation with GLAS data can be examined in Zolkos et al. (2013).

This study demonstrates the use of GLAS and Landsat data to develop regression models for the estimation of AGB at Muğla province of Turkey. The novelty of this study lies in the practice of GLAS data to estimate AGB of Mediterranean forests for the first time in Turkey where there is no airborne lidar data available. The goals of this study are (1) to create the biomass distribution map of the study area, (2) develop a method to model AGB from GLAS and Landsat integration and (3) to assess the relationship of GLAS parameters and Landsat data with biomass.

2. Study area

Muğla (36°20′–37°40′ N and 27°10′–29°50′E) is located in the southwest of Turkey covering an area around 13 km^2 (Fig. 1). The climate of this region is Mediterranean and is characterized by warm to hot, dry summers and mild to cool, wet winters. However, the spatial distributions of landforms cause local variations at the climatic characteristics. The precipitations generally depend on the middle latitude depression activities in winter that move towards east through Mediterranean fronts (Kayan, 1971). The long term annual average precipitation values of the 9 meteorological stations vary between 650 and 1230 mm (Fig. 2).

Muğla belongs to the Mediterranean phytogeographic region and 68% of the provincial area is consisted of forest land. Almost half of these forested areas have less than 10% canopy cover and are considered as degraded forest by the Turkish Ministry of Forest and Water General Directorate of Forestry (GDF) (OGM, 2006). Main species that exists in order of the coverage area are calabrian pine (*Pinus brutia*) (83%), crimean pine (*Pinus nigra*) (8%) and oak (*Quercus* sp.).

3. Data

3.1. Landsat data

Four Landsat 5 TM images cover the study area (Table 1). The selection of imagery was highly important. We used Global Land

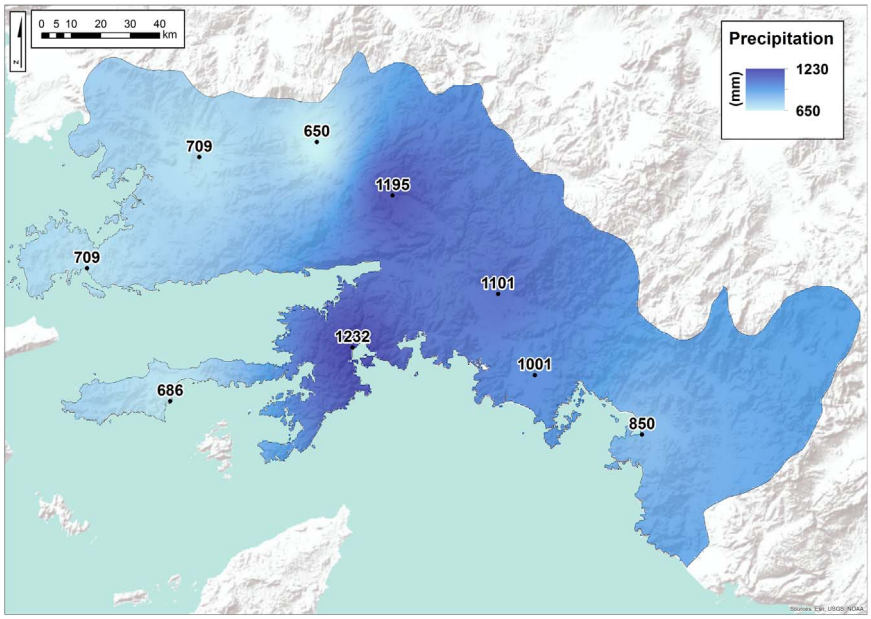

Fig. 2. The distribution of long-term annual precipitation values at Muğla for 9 meteorological stations using Inverse Distance Weighting (IDW).

Table 1
The list of Landsat TM imagery.

Landsat path–row	GLS 2010 imagery acquisition date
180–34	20–08–2009
180–35	20–08–2009
179–34	19–08–2011
179–35	20–09–2011

Survey (GLS) 2010 Landsat data sets which are cloud-free, orthorectified collections of Landsat imagery that are designed to support global land-cover and ecological monitoring (Gutman et al., 2008). All the Landsat TM imagery were calibrated and atmospherically corrected to surface reflectance by Earth Resources Observation and Science (EROS) data center using the MODIS 6S radiative transfer approach.

3.2. ICESat/GLAS data

GLAS data products GLA01, GLA06 and GLA14 of release 33 were used in this study (Fig. 3). Data was obtained from National Snow and Ice Data Center (NSIDC). Information contained in GLA01, GLA06 and GLA14 were extracted, using IDL. GLA01 and GLA06 waveforms were then linked to GLA14 on the basis of record and shot numbers. We used quality flags such as "i_FRir_qaFlag" to select cloud free shots. The laser periods and the acquisition years of the ICESat/GLAS data used in the study is listed at Table 2.

3.3. Field data

Field data were collected in 2013 and 2014. Diameter at breast height (DBH) was measured for every tree within a 10 m diameter for

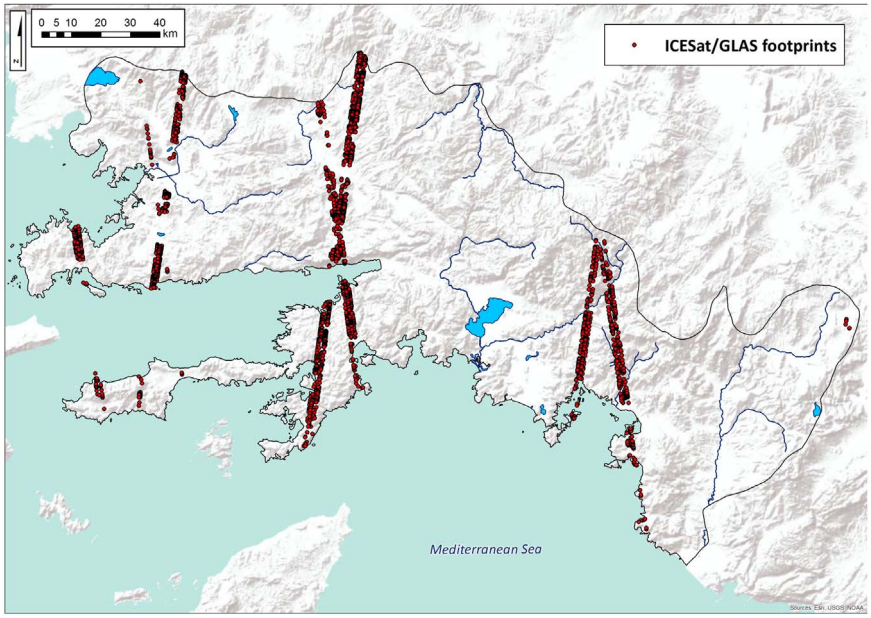

Fig. 3. The spatial distribution of GLAS footprints..

Table 2
The laser operation periods of the ICESat/GLAS data in the study.

Laser period	Start date	End date
Laser 3A	03 Oct 2004	08 Nov 2004
Laser 3C	20 May 2005	23 Jun 2005
Laser 3D	21 Oct 2005	24 Nov 2005
Laser 3E	22 Feb 2006	28 Mar 2006
Laser 3F	24 May 2006	26 Jun 2006
Laser 3G	25 Oct 2006	27 Nov 2006
Laser 3H	12 Mar 2007	14 Apr 2007
Laser 3I	02 Oct 2007	05 Nov 2007
Laser 3J	17 Feb 2008	21 Mar 2008
Laser 3K	04 Oct 2008	19 Oct 2008
Laser 2D	25 Nov 2008	17 Dec 2008
Laser 2E	09 Mar 2009	11 Apr 2009
Laser 2F	30 Sep 2009	11 Oct 2009

33 plots (Fig. 4). Eight of these were GLAS footprint locations while the other 25 plots were randomly selected. We acknowledge that the numbers of plots on the GLAS footprints are likely to be substandard. This situation was due to logistic difficulties (e.g., complexity of topography, weather conditions, refused access). Hence, we have additional randomly selected 32 plots to verify the results. All the plots were positioned using a Magellan eXplorist Pro 10 handheld GPS with a horizontal accuracy about 2–5 m.

3.4. Ancillary data

In addition to the aforementioned data sets we used ASTER DEM data is used to create slope map of the study area; stand map of the area obtained from GDF to determine the species, meteorological data of 9 stations obtained from Turkish State Meteorological Service to comprehend the climatological properties of the study area.

4. Methodology

4.1. Calculation of GLAS parameters

GLAS Visualizer for IDL obtained from NSIDC has been used to extract various parameters. These include: signal begin range offset (SigBegOff), signal end range offset (SigEndOff), centroid range increment for gaussian fits (gpCntRngOff), the peaks of first two gaussian amplitudes (gamp), centroid range offset (cntRngOff), cloud flag (FRir_qaFlag), saturation index (satNdx).

To determine the vegetation parameters from GLAS waveform various calculations need to be done. One of the crucial GLAS parameter is the height of the Gauss peak that represents the return signal from ground. The notable slope at the GLAS footprint area causes confusion of signal returning from vegetation and ground, making it hard to calculate vegetation cover height. Theoretically the peak of the first Gaussian represents the ground return for flat surfaces. However, it has been found that in some cases such as complex terrain, second Gaussian peak might represent ground return instead of the first (Rosette et al., 2008). In this study we used the waveform of either Gaussian peak # 1 or 2 whichever demonstrated the greater amplitude to determine the ground return.

Maximum vegetation height (MaxVeg) is considered to be one of the good predictors of AGB. To estimate MaxVeg the distance between signal beginning offset and the ground return has been calculated.

Various studies have shown that the height of median energy (HOME) metric is sensitive to both the vertical arrangement and density of forest canopy making it to be useful predictor of biomass. In areas with dense forest less GLAS energy is likely to reach the ground causing HOME metric to increase; conversely in open areas more energy reaches the ground and reduces HOME (Drake et al., 2002). The HOME metric we used in this study is calculated using the difference of centroid range offset and ground return. We also calculated the ratio of HOME to MaxVeg (%HOME).

All of the calculated parameters have been exported to ArcGIS 10.3 software using the location data of GLA14 data product. Removing the unnecessary footprints such as the ones that fall on the areas having more than 15° of slope, non-forest areas, having extreme values due to cloud and other conditions and, we had 2805 GLAS footprints at Muğla.

4.2. Calculation of Landsat vegetation indices

AGB estimation using vegetation indices have been in use for a long time and have been indicated to be useful in various publications (Lu,

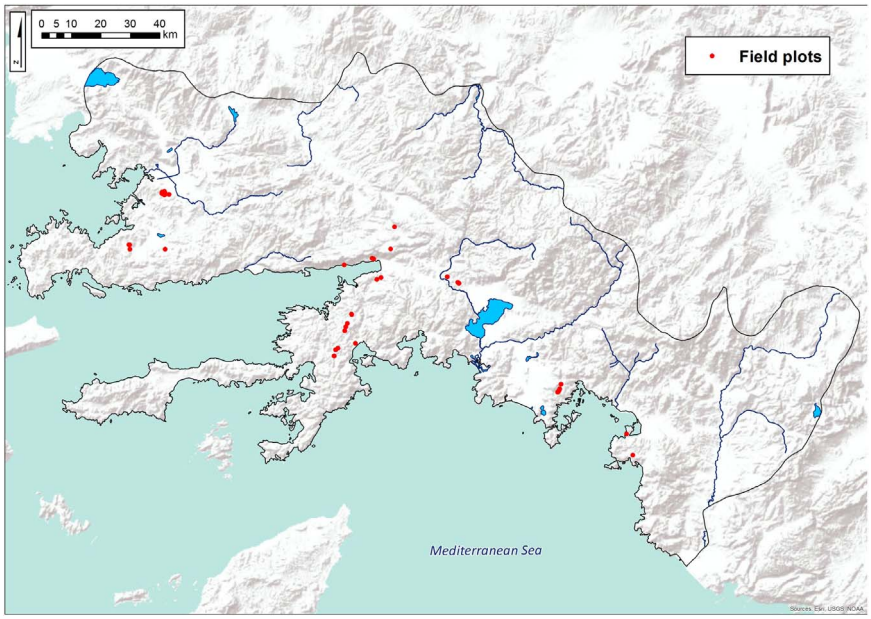

Fig. 4. The location of the field plots..

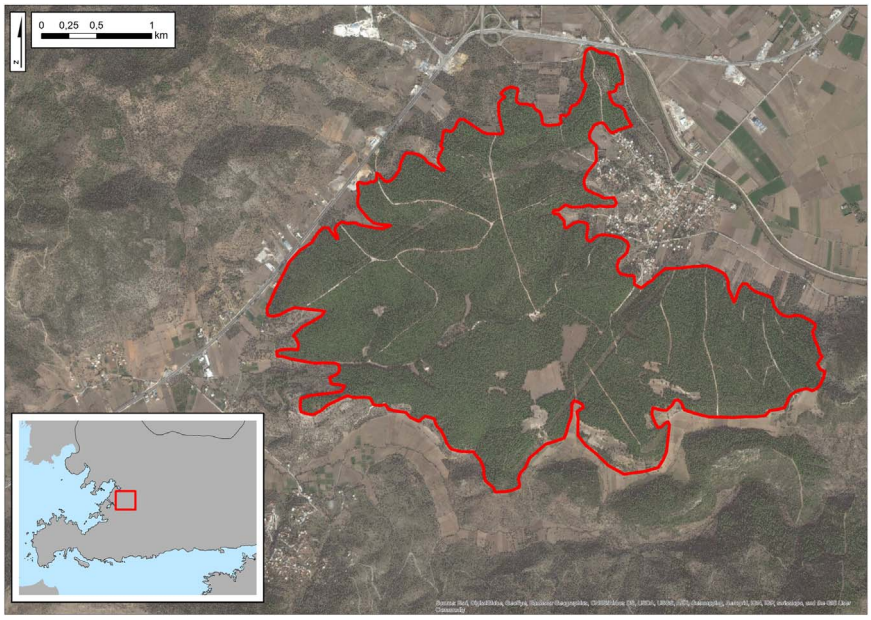

Fig. 5. Selected pilot forest area.

Table 3
Summary of the variables selection for $Model_1$. Selected model variables are shown bold..

# of variables	Variables	MSE	R^2	Adjusted R^2
2	**HOME / RH50**	59.496	**0.883**	**0.837**
3	MaxVeg / HOME / RH50	73.908	0.884	0.797

2006; Dong et al., 2003; Zheng et al., 2004). However, the correlations of these indices with AGB vary depending on many issues such as seasonality, background effects and species. In this study, we used 26 vegetation indices that are widely mentioned to be interrelated with AGB (see Appendix) to create biomass distribution map of the study area. ENVI 5.0 software is used to create the indices.

4.3. Merging ICESat/GLAS and Landsat data

We combined the Landsat indices pixel values with the GLAS footprint data using ArcGIS 10. Even though the GLAS shots coincide with one single Landsat TM pixel, they are affected from the neighbor pixels due to the size of the footprint. To reflect this effect, we used bilinear interpolation in calculation of Landsat TM pixel values on GLAS footprints.

4.4. Calculation of AGB from field data

Since almost all of the forests in the study area consisted of *Pinus brutia*, we used biomass equation of Sun et al. (1980) to calculate AGB of each individual tree (Eq. (1)).

$$AGB(kg/tree) = 0.128 \times d^{2.267} \quad (1)$$

where d is the diameter at breast height. Using all trees at the field plots, we converted the values to AGB per hectare.

Table 4
Analysis of variance for $Model_1$ (DF: degree of freedom).

	Degree of fredom	Sum of squares	Mean squares	F	Pr > F (Sig.)
Model	2	2253.043	1126.521	18.934	0.005
Error	5	297.481	59.496		
Corrected total	7	2550.524			

4.5. Modelling the relationships between AGB, GLAS and Landsat data

In order to create models to explain statistical relationships between AGB, GLAS and Landsat TM data we selected a relatively small forest area at Muğla that is considered to represent other forest areas regarding topography, geology, tree species and other forest parameters. The pilot forest area covers 607 ha and is located at the northwest of Muğla (Fig. 5).

We used multiple linear regression analysis to model the relationship between AGB values collected from field, GLAS and Landsat TM data. Multiple linear regression is a technique that estimates a single regression model with more than one outcome variable.

In the first model ($Model_1$) MaxVeg, HOME and %HOME parameters of 8 GLAS plots were used as independent variables while AGB estimates from the field data was used as dependent variables. The resulting model applied to other GLAS shots (33 shots) at the pilot forest area. Second model ($Model_2$) uses the AGB estimates of GLAS data derived from $Model_1$ as the dependent variable. The Landsat TM digital numbers of both pixel values of each band and indices are the independent variables of $Model_2$.

In multiple linear regressions, the dependent variable can be explained using all of the independent variables or only some more related ones. Various methods can be used to determine which model better explains the statistical relationship. In this study, we preferred to use the model whichever has the highest adjusted R^2. The adjusted R^2

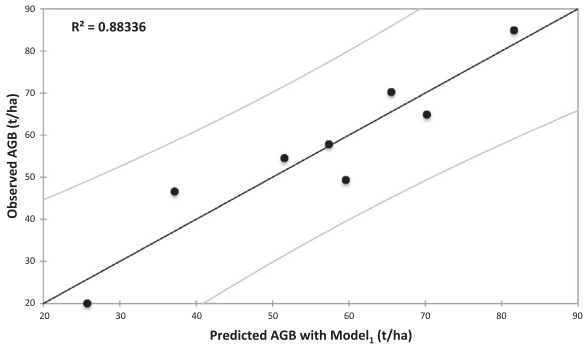

Fig. 6. Observed vs predicted AGB using $Model_1$.

Table 5
Summary of the variables selection for $Model_2$. Selected model variables are shown bold.

# of variables	Variables	MSE	R^2	Adjusted R^2
10	ARVI / EVI / MSAVI / ND53 / NDVI / B1_LANDS / B3 / B4 / B5 / B7	69.38	0.66	0.509
11	ARVI / EVI / ND32 / NDVI / TM54 / TC2 / B2 / B3 / B4 / B5 / B7	64.60	0.70	0.542
12	**ARVI/ EVI / MSAVI/ ND32 / ND54 / NDVI / B1 / B2 / B3 / B4 / B5 / B7**	60.31	**0.73**	**0.573**

is a modified version of R^2 that gives the percentage of variation explained by only those independent variables that in reality affect the dependent variable.

5. Results and discussion

5.1. $Model_1$

Examining the variable selection table, the model using HOME and %HOME has higher adjusted R^2 than the model using all the variables (Table 3). $Model_1$ explaining the AGB estimation using GLAS data is as follows:

$$AGB_{Model1} = 24.11 - 3.84 \times HOME + 2.44 \times \%HOME \quad (2)$$

Variance analysis results (Table 4) show that HOME and %HOME parameters are related with AGB having a R^2 of 0.88 (Fig. 6) and this relationship is statistically significant given the fact that the probability corresponding to the F value is lower than 0.01.

5.2. $Model_2$

$Model_2$ uses the AGB estimations using $Model_1$ for 33 GLAS shots and 32 variables obtained from Landsat TM indices and pixel values of each bands. The selected model that has the highest adjusted R^2 uses 12 variables (Table 5) and is as follows:

$$\begin{aligned} AGB_{Model2} = {} & 4185.28 + 11102.50 \times ARVI - 1150.56 \times EVI \\ & + 0.70 \times MSAVI - 1132.97 \times ND32 + 1613.33 \times ND54 \\ & - 12213.52 \times NDVI - 2.52 \times B1 - 0.94 \times B2 + 1.58 \times B3 \\ & - 0.17 \times B4 - 0.63 \times B5 - 0.04 \times B7 \end{aligned} \quad (3)$$

Table 6
Analysis of variance for $Model_2$ (DF: degree of freedom).

	Degree of fredom	Sum of squares	Mean squares	F	Pr > F (Sig.)
Model	12	3312.213	276.018	4.576	0.001
Error	20	1206.373	60.319		
Corrected total	32	4518.585			

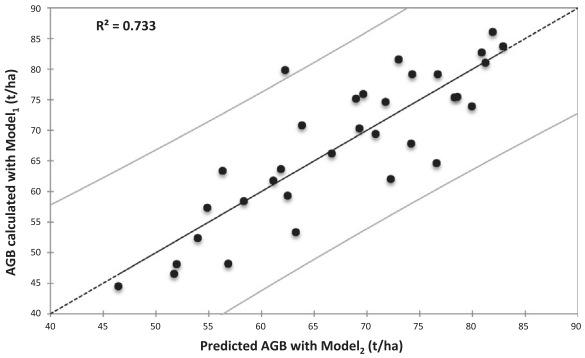

Fig. 7. AGB calculated with $Model_1$ vs predicted AGB using $Model_2$.

Variance analysis results (Table 6) show that the Landsat indices ARVI, EVI, MSAVI, ND32, ND54, NDVI and all the Landsat TM bands (except the thermal band) are related with AGB having a R^2 of 0.73 (Fig. 7) and this relationship is statistically significant given the fact that the probability corresponding to the F value is lower than 0.01.

5.3. AGB map and validation

Using the Eq. (3) and "band math" in ENVI, we have created the AGB distribution map of Muğla (Fig. 8). The non-forest areas are masked using "Disturbance Index" algorithm described on Yavaşlı et al. (2013). When the distribution of AGB analyzed in detail, it may be observed that the forests having higher AGB values are mostly situated in the center of the province. Examining the long term precipitations at the meteorological stations of the study area it may be noticed that the higher values of annual precipitations are also clustered at the same region (Fig. 2). It may be said that the AGB distribution is mostly controlled by local precipitation conditions. Even though the AGB densities vary between 0–250 t/ha, most of the forest areas have 40–100 t/ha.

To validate the results, we used field collected data of 32 randomly selected plots. It has been found that calculation of AGB using $Model_1$ and $Model_2$ allows us to explain 79% of the variability of AGB with a RMSE of ± 28.16 t/ha (Fig. 9).

6. Conclusion

Landsat and GLAS integration may be useful for AGB estimation when limitations such as funding or logistics prevent extensive data collection. This study demonstrated that remotely sensed data obtained from Landsat and GLAS can be used to estimate AGB in areas where airborne lidar data does not exist, such as Muğla. Our presented method explained 79% of the variability of AGB. Since most of the AGB

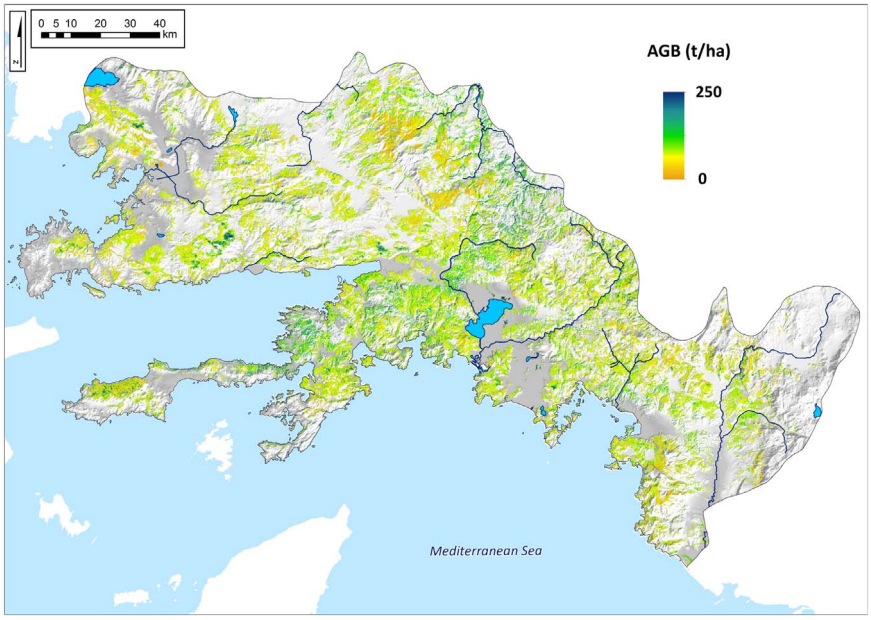

Fig. 8. AGB distribution map of Muğla.

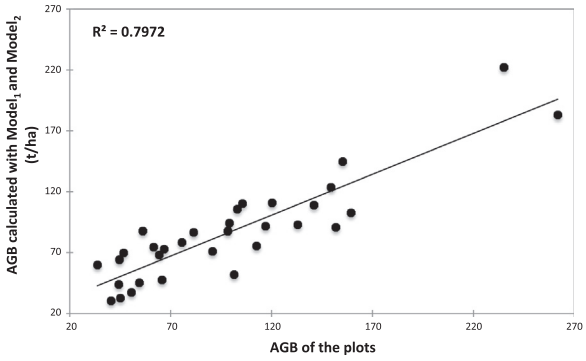

Fig. 9. Validation of AGB calculations with both models..

models based on GLAS data in literature vary between 55–74% (Zolkos et al., 2013), we suppose that our results can be considered as acceptable.

Using the models, we have created the very first biomass of distribution map of Muğla. The map shows that the higher biomass values are located at the center of the province where higher precipitation events occur. The map can also be used together with forest disturbance events such as fires or logging to estimate how much biomass is removed. This might contribute the carbon studies at the region.

The study succeeded to achieve encouraging results in estimation of AGB however we acknowledge that there are some issues that needs to be improved. The most important of these is the data collected from the field. The terrain conditions at Muğla limited the access to reach the forest areas that GLAS shots exist. We think better accuracies can be obtained if the number and of collected field data could be increased. Additionally, the field data has also AGB range between 20–90 t/ha and this might have affected the estimation error at higher biomass values. Another issue is the forest condition change during the acquisition of GLAS data and fieldwork periods. We acknowledge that this may bias the results however the lack of airborne lidar data for Turkey or more up-to-date GLAS data constrained us to use it.

Appendix A. The list of the vegetation indices used

Abbreviation	Definition	Equation
ALB	Albedo	$(tm1) + (tm2) + (tm3) + (tm4) + (tm5)+(tm7)$
ARVI	Atmospherically Resistant Vegetation Index	$\frac{nir(tm4) - 2red(tm3) + blue(tm1)}{nir(tm4) + 2red(tm3) - blue(tm1)}$
ASVI	Atmosphere Soil Vegetation Index	$\frac{2nir + 1 - \sqrt{(2nir + 1)^2 - 8(nir - 2red + blue)}}{2}$
EVI	Enhanced Vegetation Index	$2.5*\left(\frac{nir(tm4) - red(tm3)}{nir(tm4) + [6 * red(tm3)] - [7.5 * blue(tm1)] + 1}\right)$
GEMI	Global Environmental Monitoring Index	$\eta*(1 - 0{,}25\eta) - \frac{red(tm3) - 0{,}125}{1 - red(tm3)}\eta = \frac{2(nir^2 - red^2) + 1.5nir + 0{,}5red}{nir + red + 0{,}5}$
MSAVI	Modified Soil Adjusted Vegetation Index	$\frac{2nir + 1 - \sqrt{(2nir + 1)^2 - 8(nir - 2red)}}{2}$
ND32	Normalized Difference Index	$\frac{red(tm3) - green(tm2)}{red(tm3) + green(tm2)}$
ND53	Normalized Difference Index	$\frac{swir(tm5) - red(tm3)}{swir(tm5) + red(tm3)}$

ND54	Normalized Difference Index	$\frac{swir(tm5)-nir(tm4)}{swir(tm5)+nir(tm4)}$
ND57	Normalized Difference Index	$\frac{swir(tm5)-swir(tm7)}{swir(tm5)+swir(tm7)}$
NDVI	Normalized Difference Vegetation Index	$\frac{nir(tm4)-red(tm3)}{nir(tm4)+red(tm3)}$
R271	Complex Ratio	$\frac{green(tm2)-[swir(tm7)+blue(tm1)]}{green(tm2)+[swir(tm7)+blue(tm1)]}$
R327	Complex Ratio	$\frac{red(tm3)-[green(tm2)+swir(tm7)]}{red(tm3)+[green(tm2)+swir(tm7)]}$
RSR	Reduced Simple Ratio	$\frac{nir(tm4)}{red(tm3} * \frac{swir(tm5)max - swir(tm5)}{swir(tm5)max - swir(tm5)min}$
SAVI	Soil Adjusted Vegetation Index	$\frac{nir(tm4)-red(tm3)}{nir(tm4)+red(tm3)+L} * (1 + 0.5)$
TM57	Simple Ratio	$swir(tm5)/swir(tm7)$
TM54	Simple Ratio	$swir(tm5)/swir(tm4)$
TM53	Simple Ratio	$swir(tm5)/red(tm3)$
TM43	Simple Ratio	$nir(tm4)/red(tm3)$
VIS123	Visible Bands	$(tm1) + (tm2) + (tm3)$
TC1	Tasseled Cap Brightness	$0.3037(tm1)+0.2793(tm2)+0.\ 4743(tm3)+\ 0.5585(tm4)+0.5082(tm5)+0.1863(tm7)$
TC2	Tasseled Cap Greenness	$-0.2848(tm1)-0.2435(tm2)-0.5436(tm3)+0.7243(tm4)+0.0840(tm5)-0.1800(tm7)$
TC3	Tasseled Cap Wetness	$0.1509(tm1)+0.1973(tm2)+0.3279(tm3)+0.3406(tm4)-0.7112(tm5)-0.4572(tm7)$
TC4	Tasseled Cap Forth	$-0.8242(tm1)+0.0849(tm2)+0.4392(tm3)-0.0580(tm4)+0.2012(tm5)-0.2768(tm7)$
TC5	Tasseled Cap Fifth	$-0.3280(tm1)+0.0549(tm2)+0.1075(tm3)+0.1855(tm4)-0.4357(tm5)+0.8085(tm7)$
TC6	Tasseled Cap Sixth	$0.1084(tm1)-0.9022(tm2)+0.4120(tm3)+0.0573(tm4)-0.0251(tm5)+0.0238(tm7)$

References

Baccini, A., Laporte, N., Goetz, S.J., Sun, M., Dong, H., 2008. A first map of tropical Africa's above-ground biomass derived from satellite imagery. Environ. Res. Lett. 3 (4), 045011.

Boudreau, J., Nelson, R.F., Margolis, H.A., Beaudoin, A., Guindon, L., Kimes, D.S., 2008. Regional aboveground forest biomass using airborne and spaceborne LiDAR in Québec. Remote Sens. Environ. 112, 3876–3890.

Das, S., Ravindaranth, N.H., 2012. Remote sensing techniques for biomass production and carbon sequestration projects. Biomass-Assess. Handb., 178.

Davidson, E.A., Janssens, I.A., 2006. Temperature sensitivity of soil carbon decomposition and feedbacks to climate change. Nature 440, 165–173.

Dong, J., Kaufmann, R.K., Myneni, R.B., Tucker, C.J., Kauppi, P.E., Liski, J., Hughes, M.K., 2003. Remote sensing estimates of boreal and temperate forest woody biomass: carbon pools, sources, and sinks. Remote Sens. Environ. 84 (3), 393–410.

Drake, J.B., Dubayah, R.O., Clark, D.B., Knox, R.G., Blair, J.B., Hofton, M.A., Prince, S., 2002. Estimation of tropical forest structural characteristics using large-footprint lidar. Remote Sens. Environ. 79 (2), 305–319.

Dubayah, R.O., Drake, J.B., 2000. Lidar remote sensing for forestry. J. For. 98 (6), 44–46.

Fu A., Sun G., Guo Z., 2009. Estimating forest biomass with GLAS samples and MODIS imagery in northeastern China. In: Proceedings of the Sixth International Symposium on Multispectral Image Processing and Pattern Recognition. International Society for Optics and Photonics.

Ghasemi, N., Sahebi, M.R., Mohammadzadeh, A., 2011. A review on biomass estimation methods using synthetic aperture radar data. Int. J. Geomat. Geosci. 1 (4), 776.

Guo, Z.F., Chi, H., Sun, G.Q., 2010. Estimating forest aboveground biomass using HJ-1 Satellite CCD and ICESat GLAS waveform data. Sci. China Earth Sci. 53 (1), 16–25.

Gutman, G., Byrnes, R., Masek, J., Covington, S., S, Justice, C., Franks, S., Headley, R., 2008. Towards monitoring land cover and land-use changes at a global scale: the Global Land survey 2005. Photogramm. Eng. Remote Sens. 74 (1).

Kayan, İ., 1971. Gökova ve Çevresinde Fiziki Coğrafya Araştırmaları. Coğrafya Araşt. Derg., 3–4.

Kumar, L., Sinha, P., Taylor, S., Alqurashi, A.F., 2015. Review of the use of remote sensing for biomass estimation to support renewable energy generation. J. Appl. Remote Sens. 9 (1), (097696-097696).

Lefsky, M.A., Harding, D.J., Keller, M., Cohen, W.B., Carabajal, C.C., Espirito-Santo, D.B., F, Hunter, M.O., de Oliveira, R., Jr., 2005. Estimates of forest canopy height and aboveground biomass using ICESat. Geophys. Res. Lett., 32.

Lefsky, M.A., Keller, M., Pang, Y., De Camargo, P.B., Hunter, M.O., 2007. Revised method for forest canopy height estimation from Geoscience laser Altimeter System waveforms. J. Appl. Remote Sens. 1 (1), (013537-013537).

Lu, D., 2006. The potential and challenge of remote sensing-based biomass estimation. Int. J. Remote Sens. 27 (7), 1297–1328.

OGM, 2006. *Orman Varlığımız*. Ankara.

Pflugmacher, D., Cohen, W., Kennedy, R., Lefsky, M., 2008. Regional applicability of forest height and aboveground biomass models for the Geoscience Laser Altimeter system. For. Sci. 54 (6), 647–657.

Rosette, J.A.B., North, P.R.J., Suarez, J.C., 2008. Vegetation height estimates for a mixed temperate forest using satellite laser altimetry. Int. J. Remote Sens. 29 (5), 1475–1493.

Rosette, J., Cook, B., Suárez, J., North, P., Nelson, R., Los, S., 2012. Lidar Remote Sensing for Biomass Assessment. INTECH Open Access Publisher.

Roy, P.S., Ravan, S.A., 1996. Biomass estimation using satellite remote sensing data—an investigation on possible approaches for natural forest. J. Biosci. 21 (4), 535–561.

Sader, S.A., Waide, R.B., Lawrence, W.T., Joyce, A.T., 1989. Tropical forest biomass and successional age class relationships to a vegetation index derived from landsat TM data. Remote Sens. Environ. 28, (143IN1159-156IN2198).

Sarker, L.R., 2010. Estimation Of Forest Biomass Using Remote Sensing (Ph.D. dissertation). The Hong Kong Polytechnic University.

Steininger, M.K., 2000. Satellite estimation of tropical secondary forest above-ground biomass: data from Brazil and Bolivia. Int. J. Remote Sens. 21 (6–7), 1139–1157.

Sun O., Uğurlu S., Özer E., 1980. Kızılçam (Pinus brutia Ten.) türüne ait biyolojik kütlenin saptanması. Ormancılık Araştırma Enstitüsü Teknik Bülteni, Teknik Bülten Serisi No: 104. 32 pp.

Sun, G., Ranson, K.J., Kimes, D.S., Blair, J.B., Kovacs, K., 2008. Forest vertical structure from GLAS: an evaluation using LVIS and SRTM data. Remote Sens. Environ. 112 (1), 107–117.

Yavaşlı, D.D., Masek, J.G., Franks, S., 2013. Muğla İlinde 2000–2010 Yılları Arasındaki Orman Bozunum Ve Geri Kazanımının Landsat Görüntüleri İle İzlenmesi. Aegean Geogr. J. 22 (2), 91–102.

Yavaşlı, D.D., 2012. Recent approaches in above ground biomass estimation methods. Aegean Geogr. J. 21 (1), 39–51.

Zhang, Z., Ni, W., Fu, A., Guo, Z., Sun, G., Wang, D., 2008. Estimation of forest structural parameters from Lidar and SAR data. *The* International Archives of the Photogrammetry and Remote Sensing and Spatial Information Sciences, XXXVII.

Zheng, D., Rademacher, J., Chen, J., Crow, T., Bresee, M., Le Moine, J., Ryu, S.R., 2004. Estimating aboveground biomass using Landsat 7 ETM+ data across a managed landscape in northern Wisconsin, USA. Remote Sens. Environ. 93 (3), 402–411.

Zolkos, S.G., Goetz, S.J., Dubayah, R., 2013. A meta-analysis of terrestrial aboveground biomass estimation using lidar remote sensing. Remote Sens. Environ. 128, 289–298 . http://dx.doi.org/10.1016/j.rse.2012.10.017.